528

Dispersion Analysis of Polarized Bulk Reflectance Spectra of Potassium Hydrogen Succinate Monocrystal

Marta Klanjšek Gunde,[1] Vladimir Ivanovski[2] and Boris Orel[1]

[1] *National Institute of Chemistry, Hajdrihova 19, 1000 Ljubljana, Slovenia*

[2] *Institute of Chemistry, Faculty of Natural Sciences and Mathematics, Sts Cyril and Methodius University, Arhimedova 5, 1000 Skopje, Republic of Macedonia*

* Corresponding author: E-mail: marta.k.gunde @ki.si

Dedicated to Professor Dušan Hadži on the occasion of his 90th birthday

Abstract

Reflectance spectra may show very different and interesting shapes. The most interesting may be connected to Evans holes. Model calculations to reproduce this effect were done applying model dielectric function functions. When a weak oscillator appears within the frequency region of a strong one (i.e. between its TO and LO frequencies), its LO-mode frequency shifts towards higher wavenumbers. As a consequence, the oscillator strength of the corresponding weak mode becomes negative which produces a dip (Evans hole) in the reflectance spectrum. This model was successfully applied to analyze polarized reflectance spectra of potassium hydrogen succinate monocrystal in the *ac* crystal plane. The crystal symmetry was described by phenomenological model and by full symmetry consideration. The phenomenological approach applies the four-parametric model for dielectric function which allows good evaluation of asymmetric reflectance bands. A cosine dependence of oscillator strength on polarization angle was obtained for some bands, most likely due to small deviation of the crystal symmetry from orthorhombic. This is why the phenomenological approach provides good parameters for almost all phonon modes. The full symmetry consideration applies real description of dielectric tensor in the *ac* plane and the three-parameter model for dielectric function. This model could give very accurate directions of transition dipole moments, but cannot fit asymmetric bands well to measured reflectance. Both approaches describe all basic spectral features, the wide reflectance of $\nu_{as}OH$ and the two Evans holes appearing on its shoulder.

Keywords: Polarized infrared reflectance, dielectric function, dispersion relation, phonon modes, dielectric tensor, Evans hole

1. Introduction

In second half of the past century, infrared (IR) spectroscopy of crystals provided great amount of fundamental knowledge in solid state research.[1–3] The wave vector of IR light is very small compared to the edges of Brillouin zone; therefore IR phonons reveal the optical branches in its centre. For measurements in transmittance mode, oriented monocrystals must be polished in flat and very tinny slices, which is in some cases impossible to do. Many measurements were therefore done by near-normal reflection of transversal-electric (TE) polarized electromagnetic wave, or so called *s*-polarization, although investigations employing other polarizations were also performed. Such measurements require bulk monocrystals with optically flat and perfectly polished surfaces with known crystal symmetry and orientation.

Very frequently, the ionic crystals such as the simplest forms of alkali halides: NaCl, KBr, and SrJ,[1] the more complex perovskite structure of $BaTiO_3$,[4–8] rutile structure of TiO_2[9–11] and silicates (SiO_2)[12–14] were analysed. The basic objective of these studies was to obtain some data necessary to describe the mechanism of phase transitions. These ionic crystals have high specular reflectance (up to 90 %) due to the so-called "reststrahlen" phenomenon, where crystal is almost totally reflecting[3] in the vicinity of the frequencies of the normal vibrations of ions and ion groups in crystal.[3,15]

Fewer studies were performed on reflection spectra of molecular and hydrogen bonded crystals. The reflectance of such crystals is very low and by the rule remains below 40 %. The extremely low reflectance, (only few percent), was found for merkaptobenzotiazol $(C_7H_5NS_2)$

monocrystal which limited the possibilities for accurate measurements by dispersive type of spectrophotometers used in these analyses.[16–18] This low reflectance would represent a serious problem for Fourier-transform spectrophotometers, too. Thus, much care should be devoted to appropriate polishing of surfaces so that scattering of infrared light is minimized. Also, many organic hydrogen-bonded crystals have very low reflectance. However, crystals of hydrogen salts of dicarbonic acids have higher reflectance and represent therefore an exception to the rule.[19–22] One of the members of this group is potassium hydrogen succinate $KH(COOCH_2)_2$, with abbreviation KHSu. This compound is possible to be grown as a large enough single crystal (monocrystal) so that the reflectance from its surface can be measured and can easily reach around 40%.[19,23]

An impressive feature in vibrational spectrum of KHSu monocrystal is the strong and the very broad absorption band, extending from 400 to 1500 cm^{-1}. Many other bands are also present, having the origin in the vibrations of some of the molecular groups that constitute the crystal. The assignment of vibrational bands of this molecular crystal was for a long time completely unknown. The main difficulty was in the above mentioned strong broad spectral band, which assignment was doubtful, and eventually ascribed to the $\nu_{as}OH$.[24] The position of this band, its intensity and width was not possible to be obtained accurately enough from the transmittance spectra.[25] It contains additional bands, the ones appearing to be added over it and the others having the shape which is characteristic of Evans holes.[26] Transmittance spectra of tiny monocrystal slices measured in polarized light did not confirm the undoubted assignment of this band to $\nu_{as}OH$.[25] Further investigations using the attenuated total reflectance technique (ATR), confirms the band to be $\nu_{as}OH$, however, no clear data about the frequency position of the band could be obtained due to the poor spectra quality. The reason for that was the difficulty to provide a good optical contact between the monocrystal and the ATR crystal (in some literature called also internal reflection element, IRE). Further on, the problems concerning the vibrational data were tried to be solved applying Kramers-Krönig relations on bulk reflectance spectra of KHSu. It gives the possibility to determine the transversal and longitudinal optical frequencies (Ω_{TO} and Ω_{LO}, respectively) of all bands in the region 400–2000 cm^{-1}; however, no data for the corresponding dampings (damping constants) were obtained.[25]

It was assumed that dispersion analysis applying four-parametric model for dielectric function[27] enables to determine both characteristic frequencies (Ω_{TO} and Ω_{LO}), together with the corresponding dampings γ_{TO} and γ_{LO}. Since the crystal has monoclinic symmetry, the dielectric function must be treated as a tensor, which has further consequences on the reflectance spectrum analysis.[28] Parts of the results presented here, obtained in the thesis from 1982, have not been published yet.

In this article we present the old results[28] and compare them with complete dispersion analysis applying the three-parameter dispersion model, modified for monoclinic symmetry.[35–36] These results were obtained recently by applying dispersion analysis on the same (old) reflectance data. The benefits of the applied calculation methods are discussed.

2. Theory

Vibrational properties of crystals could be analysed by IR transmittance of crystal in powdered form applying KBr pellet measurement technique. This method is simple from the experimental and theoretical point of view. Samples can be prepared from practically any size of crystals and their optical quality is in most cases not important. IR absorptions occur at characteristic vibrational frequencies which could be simply read from the spectra. A transmittance spectrum presented in logarithmic scale may have additive background contributions such as baseline or interference fringes which can be, to a more-or-less good approximation, subtracted from the original spectrum. However, there are also some drawbacks of the approach. While there is no reason for orientation of crystal grains during preparation of pellets, such samples are polycrystalline and cannot give any information about direction of transition dipole moments. On the other hand if transmission measurements on slices of oriented single crystal are performed, the vibrational frequencies are equal to positions of absorbance bands only in the limit where sample thickness approaches zero.[1] Here, the optical thickness should be taken into account, being the product of the sample thickness and its refractive index. At larger thicknesses the positions of bands becomes thickness-dependent; in very thin films it is largely the effect of simple Fresnel refraction on the sample boundaries whereas in thicker films the effect of multiple reflectance of the IR beam between both boundaries prevails.[29] Both effects are very important for samples with large refractive index where strong and broad bands are not possible to analyse by usual procedures. Many of the above cases were solved by IR reflection spectroscopy of bulk samples. It requires infinitely thick samples which in reality means samples with zero transmittance over the spectral region of interest.

2. 1. Dielectric function

IR reflection spectroscopy is based on complex dielectric function which is fundamental in solid state spectroscopy.[1–3,30] As long as the response of a system to an external force is linear, it is frequency- and wave vector-dependent and it is based on linear relationship between electric displacement $\vec{D}$ and applied field $\vec{E}$:

$$\bar{D}(\bar{q},\omega) = \varepsilon(\bar{q},\omega)\varepsilon_0\bar{E}(\bar{q},\omega) =$$
$$= \varepsilon_0\bar{E}(\bar{q},\omega) + \bar{P}(\bar{q},\omega) \tag{1}$$

where $\varepsilon(q, \omega)$ is the dielectric function or relative permittivity of the solid, ε_0 is the permittivity of a vacuum (physical constant), ω is frequency, $\vec{q}$ is wave vector, and $\vec{P}$ is the polarization. $\vec{E}$, $\vec{D}$ and $\vec{P}$ are vectors and ε is a second-rank tensor. Polarization vector $\vec{P}$ is supposed to be linear combination of small displacement of charged vibrating species, giving product of local electric field and polarizability. The dielectric function, in principle, contains all possible excitations of the solid, depending on the frequency range: dielectric relaxation, lattice vibrations (optical phonons and librons), free carrier absorption, excitons and absorptions of impurities and dopants within the energy gap, valence electron polarization and interband transitions, valence band plasmon absorption.[3,30] In orthorhombic or higher crystal symmetry ε diagonalizes without off-diagonal contributions. In directions of the corresponding three principal axes the equation (1) could be described by scalar form which will be applied in following, but the consequences of crystal symmetry will be regarded later. The dielectric function is complex function

$$\varepsilon(\omega) = \varepsilon_r(\omega) + i\varepsilon_i(\omega) \tag{2}$$

which can be related to the complex refractive index $N(\omega) = n(\omega) + i\kappa(\omega)$ through:

$$\varepsilon = N^2 = (n + i\kappa)^2 = (n^2 - \kappa^2) + i(2n\kappa) \tag{3}$$

$\varepsilon_r(\omega)$ describes dispersion of the electromagnetic wave inside medium and its imaginary part, ε_i, the dielectric attenuation. Real part of complex refractive index, n, gives phase velocity of electromagnetic wave propagating in the corresponding direction within medium (c_0/n). The imaginary part, κ, is connected to the attenuation of electromagnetic wave intensity in medium, which is commonly described in Beer-Lambert form as:

$$I(x) = EE^* = I_0 e^{-\alpha x}; \quad \alpha = \frac{4\pi\kappa}{\lambda} \tag{4}$$

α is usually named absorption coefficient, x is the path length of the wave with wavelength λ in the medium. In electrostatic approximation transverse optical modes represent purely mechanical vibration of crystal lattice which is represented by harmonic oscillators with frequency Ω_{TO}. Taking into account the polarization due to local field which appears due to displacement of charges, the well-known dispersion relation is obtained:

$$\varepsilon(\omega) = \varepsilon_\infty + \sum_v \frac{\Delta\varepsilon_v \Omega_{TOv}^2}{\Omega_{TOv}^2 - \omega^2} \tag{5}$$

where Ω_{TOv} represents the frequency of v-th oscillator in the electrostatic approximation, i.e. the transverse-optical (TO) phonon. The summation runs over all vibrational modes v in particular symmetry of the crystal. ε_∞ is the high-frequency dielectric constant and represents the va-

lue at frequencies well above intrinsic lattice modes and sufficiently below the fundamental band gap. In most non-metallic solids the ε_∞ is the square of refractive index in the visible spectral region (see equation 3). $\Delta\varepsilon_v$ is the strength of v-th oscillator:

$$\Delta\varepsilon_v = \frac{N}{\varepsilon_s} \frac{\left(\sum_j e_j^* Q_{jv}\right)^2}{\sum_j M_j Q_{jv}^2} \cdot \frac{1}{\Omega_{TOv}^2} \tag{6}$$

where N is number of unit cells in unit volume, ε_s is static dielectric constant, representing the value of dielectric function at $\omega = 0$. Other parameters in the above equation are related to intrinsic properties of individual vibrations: e^* is its effective charge, Q_j its orthonormal eigenvector, M_j its reduced mass, and Ω_{TO} its transversal vibrational frequency. It follows from Equation 5 that every oscillator contributes to the static dielectric constant ε_s of the corresponding medium:

$$\varepsilon_s = \varepsilon_\infty + \sum_v \Delta\varepsilon_v \tag{7}$$

The equation (5) could be transformed to factorial form:

$$\varepsilon(\omega) = \varepsilon_\infty \prod_v \frac{\Omega_{LOv}^2 - \omega^2}{\Omega_{TOv}^2 - \omega^2} \tag{8}$$

where v runs over all oscillators (vibrations). Equation (8) is known as Kurosawa relation. It represents generalised Lyddane-Sachs-Teller equation:

$$\prod_v \left(\frac{\Omega_{LOv}}{\Omega_{TOv}}\right)^2 = \frac{\varepsilon_s}{\varepsilon_\infty} \tag{9}$$

The dielectric function given in the equation (5) or (8), describes the electromagnetic wave in a medium in direction of selected principal axes of the dielectric tensor. It has poles at $\omega = \Omega_{TO}$ and crosses zero at $\omega = \Omega_{LO}$, which are the frequencies of transverse (TO) and longitudinal (LO) optical phonon modes, respectively.

Combining equations (5) and (8) one could obtain:

$$\Delta\varepsilon_v = \left(\Omega_{LOv}^2 - \Omega_{TOv}^2\right) \cdot \frac{\varepsilon_\infty}{\Omega_{TOv}^2} \cdot \prod_{\mu \neq v} \frac{\Omega_{LO\mu}^2 - \Omega_{TOv}^2}{\Omega_{TO\mu}^2 - \Omega_{TOv}^2} \tag{10}$$

This equation shows that the oscillator strength is proportional to , which is called the LO-TO splitting. This phenomenon is responsible for removal of the degeneracy between the LO and TO phonons at the Brillouin zone centre. The splitting is the largest in polar solids. In homopolar crystals, such as Si or Ge, no polar interactions appear. In such crystals, $\Omega_{LO} = \Omega_{TO}$ and $\varepsilon_s = \varepsilon_\infty$.[3]

The anharmonic effects are described by damping γ which is applied to all vibrational modes. In this way equation (5) becomes:

$$\varepsilon(\omega) = \varepsilon_\infty + \sum_\nu \frac{\Delta\varepsilon_\nu \Omega_{TO\nu}^2}{\Omega_{TO\nu}^2 - \omega^2 + i\omega\gamma_{TO\nu}} \qquad (11)$$

and equation (8) is transformed to:

$$\varepsilon(\omega) = \varepsilon_\infty \prod_\nu \frac{\Omega_{LO\nu}^2 - \omega^2 + i\omega\gamma_{LO\nu}}{\Omega_{TO\nu}^2 - \omega^2 + i\omega\gamma_{TO\nu}} \qquad (12)$$

The γ_{TO} and γ_{LO} are dampings of TO and LO phonons, respectively. Each oscillator could be described by three parameters, $\Omega_{TO\nu}$, $\gamma_{TO\nu}$ and $\Delta\varepsilon_\nu$; therefore the corresponding dispersion relation (equation 11) is called the three-parametric dispersion relation. The relation (12) has four parameters for each oscillator, $\Omega_{TO\nu}$, $\gamma_{TO\nu}$, $\Omega_{LO\nu}$, $\gamma_{LO\nu}$, therefore it is called four-parametric dispersion relation. If $\gamma_{TO} = \gamma_{LO}$, the equations (11) and (12) are identical.

2. 2. Model calculation

The IR reflection spectroscopy is usually performed applying transverse-electric (TE) polarization. Here, the polarization is perpendicular to the plane of incidence. The sample is characterized by frequency dependent complex refractive index, which is related to dielectric function by means of equation (3). In the normal (and as approximation for near-normal incidence) the specular reflection is:

$$R = \frac{(n-1)^2 + \kappa^2}{(n+1)^2 + \kappa^2} \qquad (13)$$

Combining this equation with (2), (3) and applying three- or four-parametric dispersion relation (eq. (11) or (12), respectively), the reflectance of the investigated medium can be modelled and calculated. In this way the model calculation was done to show the shapes of reflectance spectrum for some selected values of the parameters.[29] The results obtained employing the four-parametric dispersion relation are presented here.

A single polar vibration causes a reflectance band. In harmonic case ($\gamma_{TO} = \gamma_{LO} = 0$) no light can propagate at any frequency between Ω_{TO} and Ω_{LO}. Therefore, this light completely reflects ($R = 1$), which is known as "reststrahlen" phenomenon. However, such a case is never strictly true while all real oscillators have certain damping. It diminishes the reflectance from 1, as shown in Figure 1a. The damping could be associated with inflection point at corresponding mode frequency, Ω_{TO} or Ω_{LO}. The maximum of reflectance is located somewhere between Ω_{TO} and Ω_{LO}. The shape of the reflectance band is never symmetric. Equal γ_{TO} and γ_{LO} gives equal shape of the reflectance band. It is helpful to consider γ_{TO} and γ_{LO} as the inclination of the reflectance at Ω_{TO} and Ω_{LO}, respectively. When $\gamma_{TO} = \gamma_{LO} = 0$ the reflectance rises to 100 % at both Ω_{TO} and Ω_{LO} and remains that high all between. In such a case, ε_r has a pole (infinite value) at Ω_{TO} and crosses zero at Ω_{LO}. When a certain damping is introduced, the reflectance is lower than 100%, ε_r drops from infinity and ma-

kes ε_i to obtain values different from zero. When dampings are sufficiently small, ε_r is below zero between Ω_{TO} and Ω_{LO} (Figure 1b). For oscillators with $\gamma_{TO} = \gamma_{LO}$ the ε_i, the dielectric attenuation function, has a symmetric shape and its band maxima are exactly at Ω_{TO} (Figure 1c).
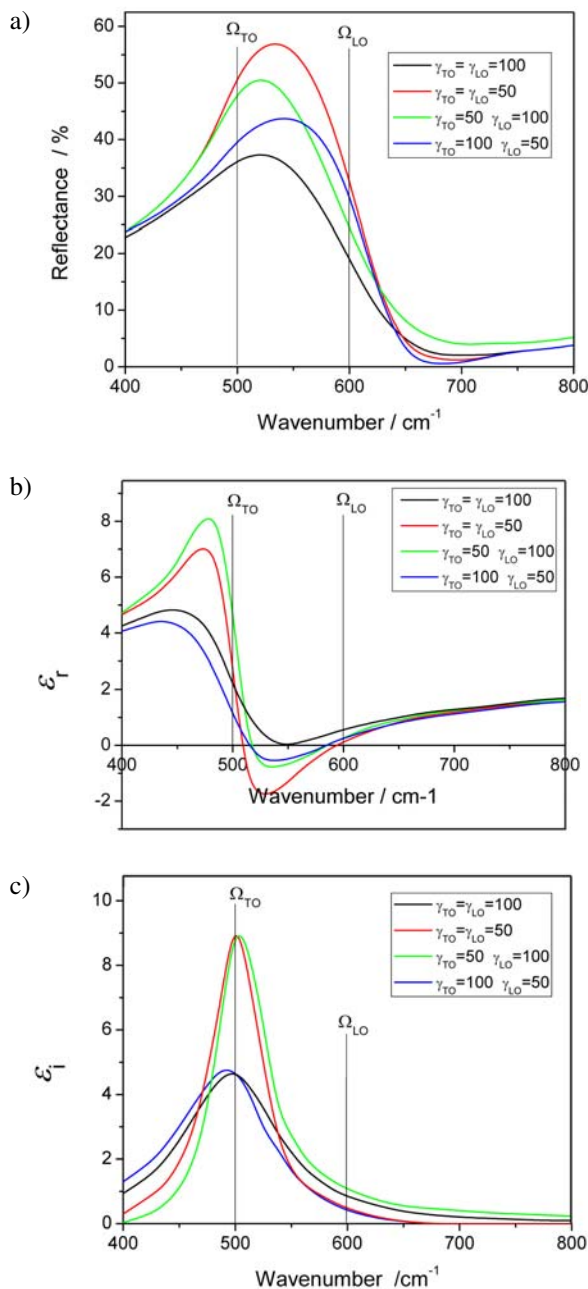

Figure 1. Single polar vibrational mode in reflectance (a), ε_r (b) and ε_i (c) as calculated applying equations 12, 13, 2 and 3 using $\varepsilon_\infty = 2$. Other parameters are shown on the pictures in cm^{-1}; $\varepsilon_\infty = 2$.

Two separated polar modes gives two separate reflectance peaks (Figure 2). The reflectance is not additive; the position of smaller peak may be influenced much due to vicinity of a stronger one. However, the dielectric atte-

nuation function ε_i is additive and gives maxima at TO frequencies of both peaks. It is worth to be noted here, that it is: $\Omega_{TO1} < \Omega_{LO1} < \Omega_{TO2} < \Omega_{LO2}$.
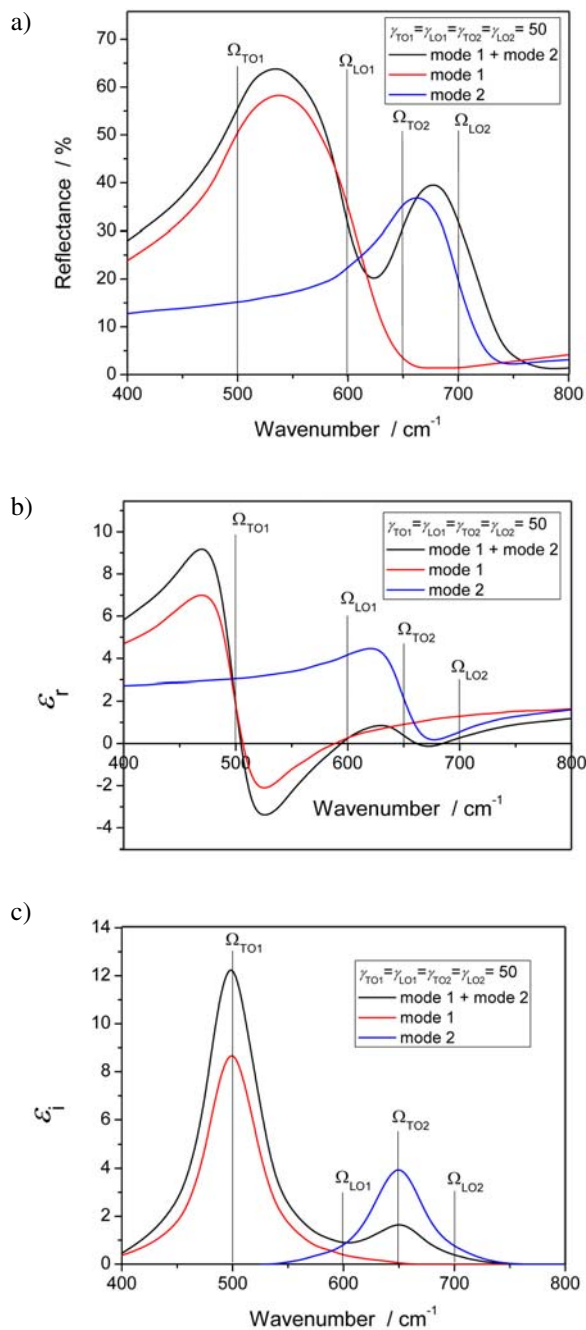
a)

b)

c)

Figure 2. Two polar modes in reflectance (a), ε_r (b) and ε_i (c) as calculated applying equations 12, 13, 2 and 3 for $\varepsilon_\infty = 2$. Other calculation parameters (in cm⁻¹) are shown on the pictures.

The situation becomes complicated if vibrations appear in the same frequency region. Such situation is represented here by two modes where one of them have much higher strength than the other ($\Delta\varepsilon_2/\Delta\varepsilon_1 << 1$). The harmo-
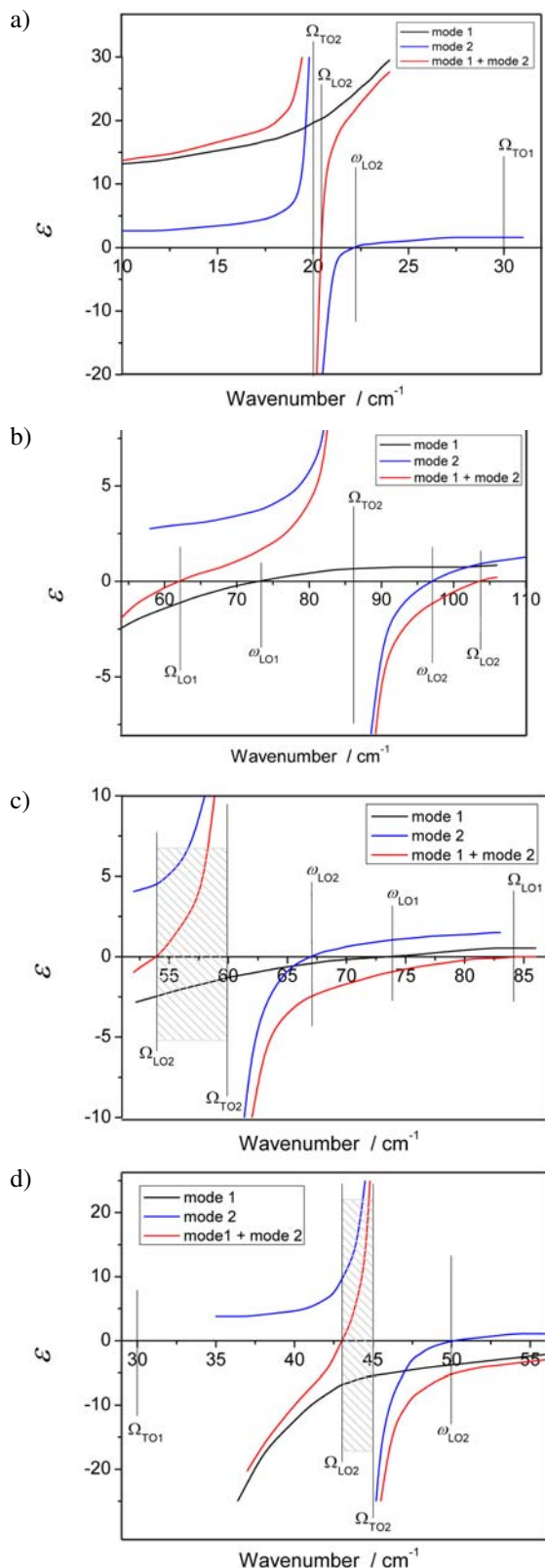
a)

b)

c)

d)

Figure 3. Coupling of strong harmonic oscillator (mode 1, $\Delta\varepsilon_1 = 10$, $\Omega_{TO1} = 30$ cm⁻¹) with weak one (mode 2, $\Delta\varepsilon_1 = 0,5$) which is located outside the strong vibration at 20 cm⁻¹ (a) and 85 cm⁻¹ (b). The Evans hole is obtained when the weak oscillator is located at 45 cm⁻¹ (b) and 85 cm⁻¹ (c). The region of Evans hole where $\Omega_{LO2} < \Omega_{TO2}$ is marked.

nic approximation was applied (equation 5) which assures additivity of dielectric function and describes TO and LO frequencies as its poles and zeros, respectively. For convenience the positions of single uncoupled oscillators were denoted by ω_{TOi} and coupled by Ω_{TOi}, i = 1,2. The parameters of strong oscillator were $\Delta\varepsilon_1 = 10$, $\omega_{TO1} = 30$ cm^{-1}. The weak oscillator with $\Delta\varepsilon_2 = 0,5$ was ascribed on four
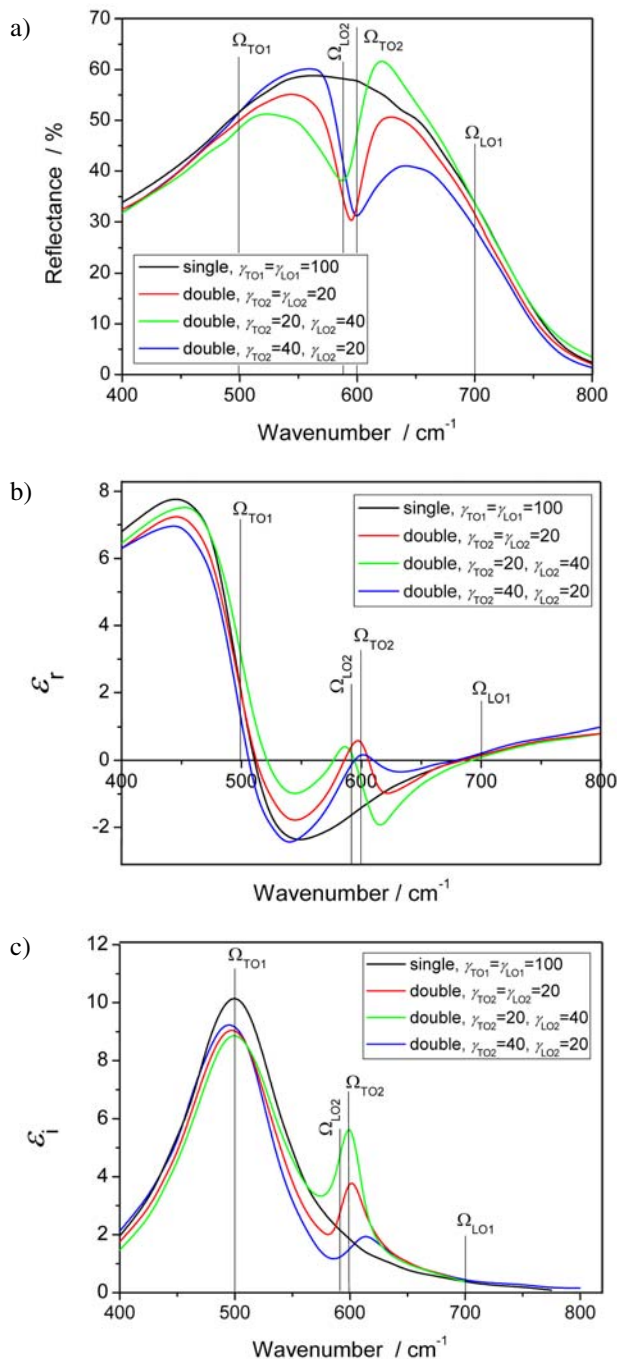

a)

b)

c)

Figure 4. Coupling of a weak polar vibrational mode with a strong one when the former is located within the frequency region of the strong mode. Reflectance (a), ε_r (b) and ε_i (c) were calculated applying equations 12, 13, 2 and 3 using $\varepsilon_\infty = 2$. The parameters of the two modes (in cm^{-1}) are shown on the pictures.

different ω_{TO1} positions, below ω_{TO1} ($\omega_{TO2} = 20$ cm^{-1}, Fig. 3a), within the region where ε_1 is negative ($\omega_{TO2} = 45$ cm^{-1}, Fig. 3b, $\omega_{TO2} = 60$ cm^{-1}, Fig. 3c), and outside this region ($\omega_{TO2} = 86$ cm^{-1}, Fig. 3d). The common dielectric function was obtained by adding the corresponding curves for single polar vibrations as followed by equation 5. The results are shown in Figures 3. In all studied cases $\omega_{TOi} = \Omega_{TOi}$, confirming that common dielectric function cannot move the poles of individual contributions. However, it cannot be true for zeros, $\omega_{LOi} \neq \Omega_{LOi}$. Interestingly, the frequencies of coupled modes always follows the rule Ω_{TO}, Ω_{LO}, Ω_{TO}, Ω_{LO}, ... Therefore, the dielectric function has repeating sequence where a pole is always followed by a zero. The individual frequencies of coupled modes were ascribed to both modes according to their uncoupled frequencies. This procedure gives that a weak polar mode which is located on the frequency region of the stronger one, couples with the strong vibration giving $\Omega_{TO2} > \Omega_{LO2}$.

Changing the LO phonon mode frequency of a weak oscillator placed in frequency region of a strong one in a real case (where dampings are taken into account) gives an interesting spectral feature in reflectance spectra (Figure 4). It is very likely that it could be used to describe the Evans hole.[26] It considers a mode with narrow vibrational energy placed in a continuum of vibrational levels, produced by a strong mode. The energy levels in the region of narrow band are displaced and produce a hole instead of a peak. The effect is frequently observed in IR spectra of samples with complex molecules.[31] The model presented in Figure 3 show that such a phenomenon is connected with regions where the $\varepsilon_r < 0$, i.e. between TO and LO frequencies. In such a case the dielectric function raises due to the weak oscillator; it causes drop of reflectance, which forms a narrow hole in the reflectance peak of the strong polar mode. The detailed shape of Evans hole depends on damping (Figure 4).

2. 3. Crystal Symmetry Considerations

The equation (1) which is applied together with time-dependent Maxwell equations to derive dispersion relations (5) and (8). When written in scalar form it describes well the real situation only in crystals with cubic crystal symmetry. In general, $\vec{E}$, $\vec{D}$ and $\vec{P}$ are vectors and ε is second-rank tensor. All equations from the last paragraph are therefore written for a selected principal direction of tensor ε. In crystals with orthorhombic symmetry or higher, the principal axes of the dielectric tensor ε coincide with crystallographic axes. Infrared light with polarization along one of crystallographic axes therefore induce normal vibrations with this symmetry and the parameters of the dispersion relation (10, 12) describe the properties of normal modes propagating along this principal axis. In cubic crystals the tensor reduces to a scalar since the tensor is diagonal and all the diagonal elements are equal. Therefore, all three principal axes give the same dielectric

tensor ε. In orthorhombic crystals, the transition dipole moments of the modes are oriented along one of the principal axes, thus being linearly independent, and the dielectric tensor is diagonal with different values for the tensor elements.

In monoclinic crystals only one of the principal axes of dielectric tensor coincides with a crystallographic direction; it describes normal vibrations of A_u symmetry type which will be further referred in the text as A_u-modes. This direction is denoted here as *y* and is parallel to crystallographic axis *b*. All other normal coordinates of B_u symmetry type (B_u-modes) are linearly independent on A_u modes and have transition dipole moments arranged in arbitrary direction in the *xz*-plane. The principal axes *x* and *z* of the dielectric tensor are frequency-dependent, i.e. for every IR active mode their orientation is different, and both axes lie in the *ac* crystal plane.[32,33] On the other hand, the *a* and *c* axes are not perpendicular to each other in crystals with monoclinic symmetry, meaning that one of the principle axis can be oriented along a crystallographic one by chance, but never both. Transition dipole moments of all B_u modes have therefore arbitrary directions in *ac* crystal plane. Dispersion of electromagnetic wave with polarization vector parallel to *ac* crystal plane was described here by two approaches, a phenomenological[29] and precise one.[34–38]

If electromagnetic wave is polarized parallel to the transition dipole moment of a selected B_u normal vibration, the oscillator parameters of this mode define the corresponding phonon mode. If three-parametric description (equation 10) is applied, it defines the frequency Ω_{TO}, damping γ_{TO} and oscillator strength $\Delta\varepsilon$ of this mode; if four-parametric dispersion relation is used for ε (equation 12), frequency and damping of TO- and LO-phonon modes, Ω_{TO}, γ_{TO}, Ω_{LO}, γ_{LO}, are obtained, respectively. It is reasonable to assume that the contribution of the selected mode to the dispersion of wave is the largest when polarization is perpendicular to its transition dipole moment and diminishes to a minimum when polarization is perpendicular to it. In general, arbitrary polarization direction within *ac* crystal plane gives oscillator parameters of all B_u normal modes. If the direction is found where oscillator strength of a selected mode is minimal, then the parameters obtained perpendicular to this direction are the values of the vibrational mode.

From the mentioned above follows that the dielectric tensor can be diagonalized for each frequency at a time, so that performing the fit, the frequency, together with the damping and the oscillator strength can be obtained. This is however only an approximation, since the dielectric tensor is not diagonal for the other transition dipole moments, and in order to perform dispersion analysis along the principal axis, the dielectric tensor must be diagonal in the whole frequency range i.e. for all the modes at the same time.

This obstacle has been solved in the late 70's by Belousov and Pavinich,[35] and further on improved by Emslie
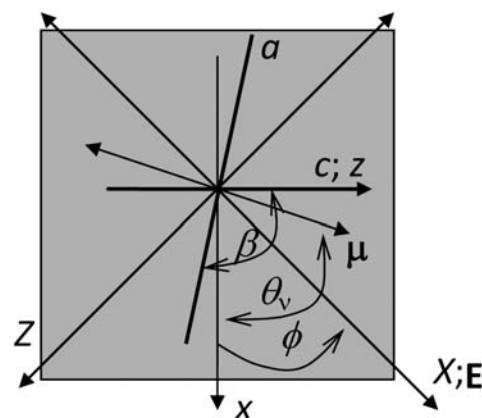

Figure 5. Measurement geometry applied for recording the B_u symmetry type modes as viewed along the *b* crystal axis, ($\beta \neq 90°$). Internal coordinate system fixed to the crystal is denoted by (*x, y, z*) and the external coordinate system (*X,Y,Z*) is fixed to the polarization vector *X* (the external electric field vector **E**). Δ is the transition dipole moment of the ν-th oscillator, and θ_ν is the angle between the transition dipole moment and the internal coordinate *x*-axis. The polarization angle is represented by angle ϕ.

et al.[36] Some recent papers on the application and modification of this dispersion analysis method can be found in refs.[34,37,38] The basis of this approach is the following.

The dielectric tensor axis (small *x*, *y* and *z* letters, cf. Fig. 5) are fixed to some internal characteristic directions of the single crystal, like its crystal axes which are further related to the morphology of the crystal. This enables to make correspondence between the crystal morphology and the orientational dependence of the optical, dielectric and vibrational properties. The *n*-th transition dipole moment encompasses angle θ_n with the *x* direction of the internal coordinate system. The dielectric tensor expressed through the internal coordinates can be written through the equation[34,37]

$$\widetilde{\varepsilon}_{x,z} \equiv \begin{pmatrix} \widetilde{\varepsilon}_{xx} & \widetilde{\varepsilon}_{xz} \\ \widetilde{\varepsilon}_{xz} & \widetilde{\varepsilon}_{zz} \end{pmatrix} = \begin{pmatrix} \varepsilon_{\infty xx} & \varepsilon_{\infty xz} \\ \varepsilon_{\infty xz} & \varepsilon_{\infty zz} \end{pmatrix} +$$

$$+ \sum_{\nu=1}^{N} \begin{pmatrix} \cos^2\theta_\nu & \cos\theta_\nu\sin\theta_\nu \\ \cos\theta_\nu\sin\theta_\nu & \sin^2\theta_\nu \end{pmatrix} \frac{\Omega_{TO\nu}^2 \Delta\varepsilon_{TO\nu}}{\Omega_{TO\nu}^2 - \omega^2 - i\omega\gamma_{TO\nu}} \tag{14}$$

where apart from the other three vibrational parameters, the angle θ_n representing the angle between the transition dipole direction and the *x* axis is now present as a parameter.

We consider here normal incidence reflectance on the *ac* crystal surface. The polarization vector (coinciding with the direction of the electric field vector) was rotated by rotating the crystal sample around *b* crystal axis. This way the transition dipole moment of each mode was triggered depending on the angle ϕ between the electric field vector and the internal coordinate *x* axis. The external and the internal coordinate systems share the same *y* axis,

which corresponds to the *b* crystallographic axis. In order to be able to further model the reflectance function and perform dispersion analysis with it, the dielectric tensor expressed in internal coordinates has to be transferred into external, since the reflectance is connected with the electric field response of the investigated system. To do so, a unitary transformation using rotational matrix is performed,

$$\widetilde{\varepsilon}_{X,Z}(\phi) = \begin{pmatrix} \cos\phi & \sin\phi \\ -\sin\phi & \cos\phi \end{pmatrix} \begin{pmatrix} \widetilde{\varepsilon}_{xx} & \widetilde{\varepsilon}_{xz} \\ \widetilde{\varepsilon}_{xz} & \widetilde{\varepsilon}_{zz} \end{pmatrix} \begin{pmatrix} \cos\phi & -\sin\phi \\ \sin\phi & \cos\phi \end{pmatrix} \quad (15)$$

It has to be pointed out that two complex reflectance amplitudes $\widetilde{r}_{XX}$ and $\widetilde{r}_{ZZ}$ the expressions of which can be found in ref.[35] will now determine the reflectance R_X, so that the reflectance for a particular polarization angle ϕ will be given with equation,

$$R_X(\phi) = \left| \widetilde{r}_{XX} \right|^2 + \left| \widetilde{r}_{XZ} \right|^2 \quad (16)$$

3. Experimental and Calculations

The potassium hydrogen succinate (COOH–(CH$_2$)$_2$–COOK, abbreviation KHSu) crystallizes in monoclinic symmetry with space group C_{2h}^6.[19,25] The angle between *a* and *c* crystallographic axes is $\beta = 90.8°$. The projection of the conventional unit cell on *ac* crystal plane is shown in Figure 6. Each "molecule" has potassium cation and succinate anion – a chain of OOC(CH$_2$)(H$_2$C)COOH. The hydrogen in COOH forms hydrogen bond between neighbour molecular units. These hydrogen atoms lie on twofold axes. The centres of C$_4$O$_4$H$_4$ molecules represent centres of inversion. All other atoms are on general positions. The hydrogen bond is 0.245 nm in length, C=O bond 0.123 nm, and C–OH 0.130 nm. The part of the chain associated with hydrogen bond is parallel to *ac* crystal plane.
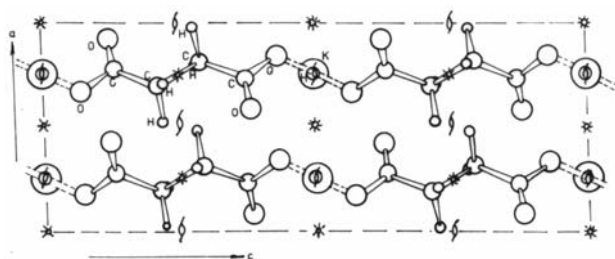

Figure 6. The primitive cell of KHSu crystal (projection of molecular structure on *ac* crystal plane.[25]

The KHSu belongs to compounds with very short hydrogen bond (less than 0.25 nm). The proton appears on one of the symmetry elements of the crystal's space group. Thus the molecular species on both sides of hydrogen bond are equal. Such hydrogen bond is symmetric.

The internal vibrations of KHSu give rise to two IR active types, A$_u$ and B$_u$, having transition dipole moments along *b* crystal axes and in *ac* crystal plane, respectively.

The IR reflectance spectra were measured with a Perkin-Elmer 180 spectrophotometer equipped with wire grid polarizer at approximately 6° incidence angle. The resolution was 5 cm^{-1}. The reflection spectra from *ac* crystal plane were measured in transverse electric (TE) polarization at seven angles with respect to *c* crystal axis, $\phi = 0°, 20°, 50°, 70°, 90°, 130°, 160°$. The angle ϕ was varied by rotating the sample around the *b* crystal axis. The spectra were measured in the 400–2000 cm^{-1} spectral region.

The data shown here were reproduced from data collected in thesis accomplished in 1982.[29] Experimental points are given here as an output of matrix-dot line printer which was applied to print out the experimental and calculated spectra. Unfortunately, the measured reflectance is given in two decimal places only and the authors did not found better data. Therefore the analysis based on equations 14–16 was performed on these old measurements.

In phenomenological approach all measured reflectance spectra were fitted with four-parametric dispersion relation (equation 12), calculating reflectance spectrum applying equations 2, 3 and 13. Each spectrum contains 9–12 reflectance peaks of different shapes, thus 36–48 oscillator parameters were used to fit entire spectrum at selected polarization angle ϕ. The model calculations show that the oscillator parameters influence reflectance curve within limited frequency range, therefore at least some of them were regarded as more-or-less independent. The high frequency dielectric constant ε_∞ fits the reflectance at frequencies above the highest reflectance peak and represents additional parameter. All the fitting parameters were adjusted manually according to visual tolerance to the corresponding measured spectrum. This way four parameters (frequency and damping of TO- and LO-phonons) were obtained for each peak recorded in reflectance spectrum at selected ϕ and the corresponding ε_∞. The oscillator strengths $\Delta\varepsilon_\nu$ were calculated for each oscillator ν in all measured polarization directions ϕ by equation 5. Then the oscillator data of vibrational modes and direction of the corresponding transition dipole moment were determined according to the dependence of $\Delta\varepsilon_\nu$ on the angle ϕ.

The dispersion analysis taking into account the monoclinic crystal symmetry as described in refs.[34–38] was performed applying equations (11), (15) and (16) on the "old" reflectance data. In order for the best fit to be obtained, at least three reflectance spectra have to be fitted simultaneously.[39] This is one characteristic feature in the dispersion analysis of reflectance spectra of monoclinic crystals. For obtaining the vibrational parameters in higher symmetry crystals (orthorhombic or higher) the fitting is performed on one spectrum at a time. However in the literature it is stated that larger number of spectra fitted simultaneously will lead to better results, thus, four reflec-

tance spectra (instead of minimum three) at $\phi = 0°$, 50°, 90° and 130° were used for that purpose. Non-linear fitting procedure employing Levenberg-Marquard algorithm was performed using a purposely written program in Mathematica 5.2 program package.[40]

4. Results and Dicsussion

4. 1. Phenomenological Approach

The phenomenological fitting procedure gives very good approach to measured reflectance in all directions ϕ (Figure 6). The dependence of oscillator frequencies on polarization angle ϕ is shown in Figure 7. The broad reflectance band due to $v_{as}OH$ starts with large LO-TO splitting at $\phi = 0°$ and vanishes completely at $\phi = 90°$. The bands at 910 and 1210 cm^{-1} start to appear at a particular angle ϕ inside the region between both phonon frequencies of the $v_{as}OH$ mode. In such a case, the corresponding LO-frequency is smaller than the corresponding TO one (see Figure 7b).
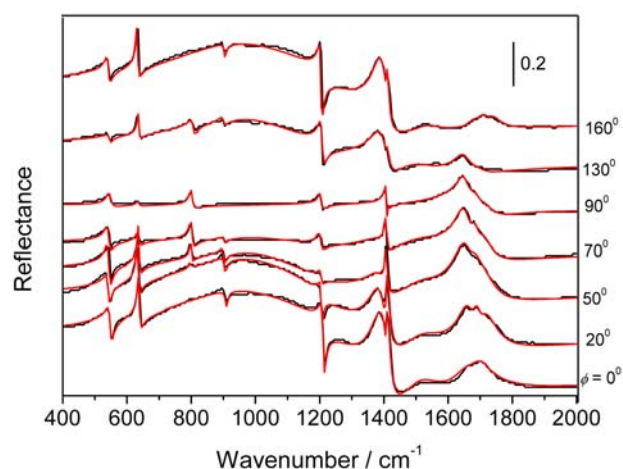
Figure 6. Best fit to the experimental reflectance with polarization at specified ϕ values applying the phenomenological approach. Black lines represent measured data and red lines calculated reflectance.

The obtained best fitting parameters for all oscillators were applied to calculate the corresponding oscillator strength parameter $\Delta\varepsilon$. Some of them show cosine dependence on polarization direction ϕ (Figure 7). The direction of transition dipole moment of the corresponding modes was set to be at the maximum value of $\Delta\varepsilon$. The fitting parameters of the oscillator at this ϕ were chosen to be the parameters of the vibrational mode. However, some oscillators do not resemble any acceptable phenomenological dependence of $\Delta\varepsilon$ on ϕ. For these modes the phenomenological approach cannot predict any well-defined mode parameters. The approximate mode parameters were chosen at maximum of the corresponding $\Delta\varepsilon (\phi)$ where some

approximation / judgments were applied. The corresponding data are collected in Table 1. The band assignment was done according to the literature data[25].
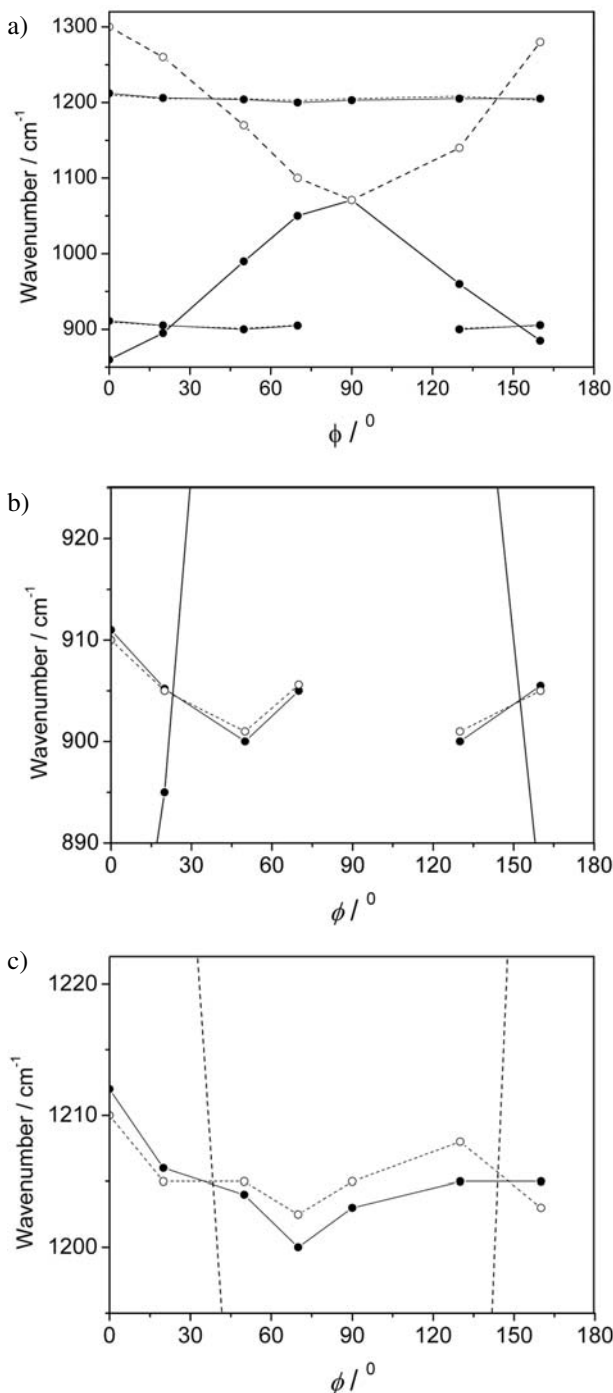
Figure 7. The dependence of oscillator frequencies on polarization angle ϕ. Spectral region of $v_{as}OH$ vibrational mode is shown only. The TO-oscillator frequencies are represented by solid circles and full line and LO-oscillator frequencies by broken line. The results were obtained by fitting the four-parametric dielectric function to measured reflectance (see Fig. 6). Frequencies of all oscillators in the considered spectral region are presented in (a). The parameters of Evans holes at 911 and 1210 cm^{-1} are shown in enlarged form in (b) and (c), respectively.

Table 1. The B_u-phonon mode parameters of KHSu monocrystal obtained by phenomenological analysis of fitting results: frequencies and dampings of TO and LO phonon modes (Ω_{TO}, γ_{TO}; Ω_{LO}, γ_{LO}, respectively), corresponding oscillator strength ($\Delta\varepsilon$), direction of transition dipole moment (θ) and asymmetry (γ_{LO}/γ_{TO}).

assignment	Ω_{TO} (cm⁻¹)	γ_{TO} (cm⁻¹)	Ω_{LO} (cm⁻¹)	γ_{LO} (cm⁻¹)	θ (°)	$\Delta\varepsilon$	γ_{LO}/γ_{TO}
*	1705	40	1710	60	70	0,004	1,5
*	1676	45	1699	45	50	0,014	1
νC=O	1642	55	1667	45	50	0,086	0,82
*δOH	1505	100	1518	150	0	0,014	1,5
δCH$_2$	1405	8	1408	11	70	0,006	1,38
*νC-O	1375	75	1402	30	0	0,021	0,40
*wag CH$_2$	1212,5	17	1210	6	0	–0,004	0,35
νC-C	911	11	910	9	0	–0,056	0,82
ν_{as}OH	860	340	1300	390	0	3,320	1,15
*rock CH$_2$	800	10	802	13	90	0,011	1,30
δOCO	635	6	639	8	0	0,122	1,33
πC=O	545	15	549	10	0	0,128	0,67

* The applied methodology did not give well defined direction of the transition dipole moment. The data corresponds to the direction with maximal $\Delta\varepsilon(\phi)$.
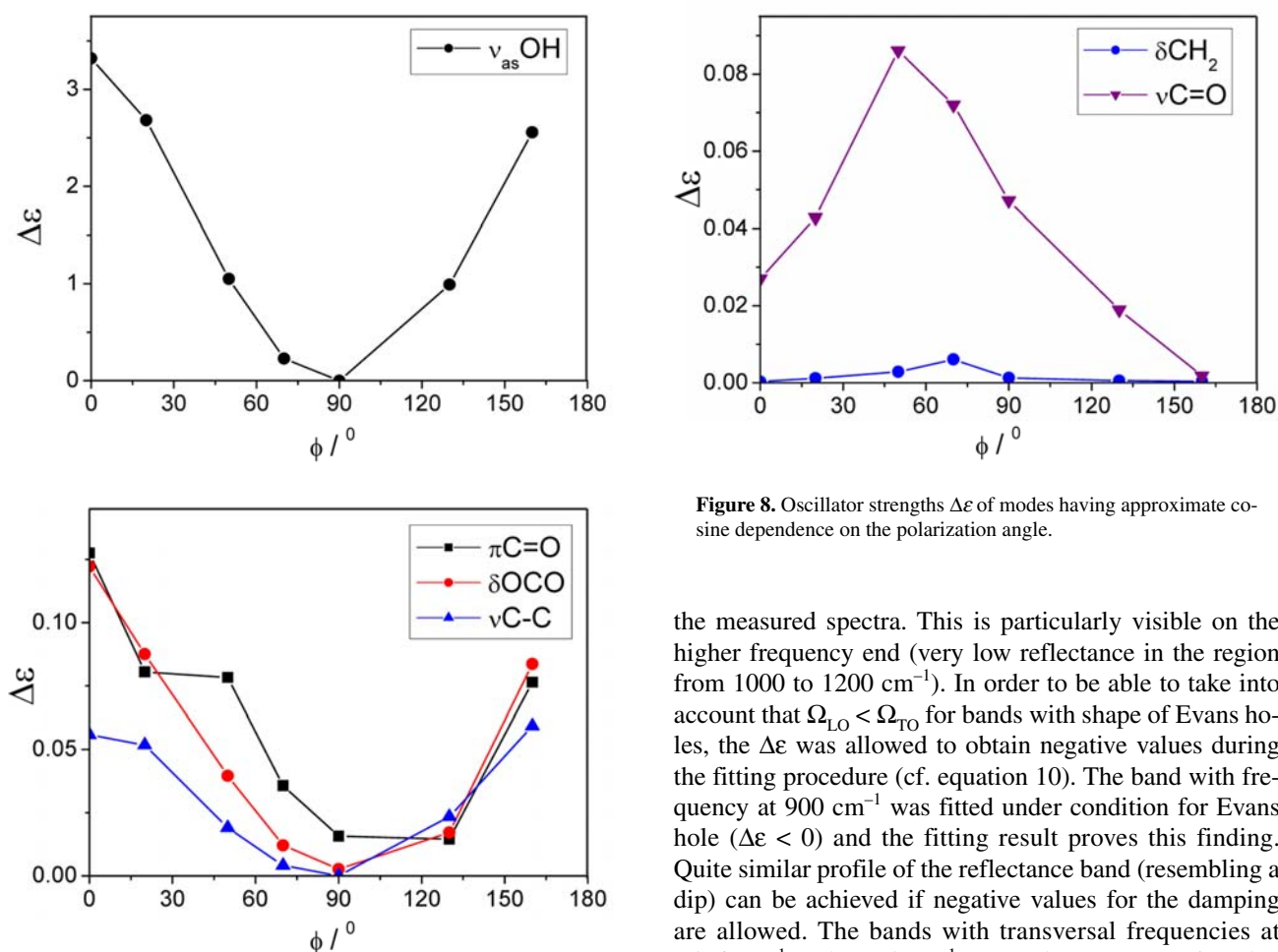

Figure 8. Oscillator strengths $\Delta\varepsilon$ of modes having approximate cosine dependence on the polarization angle.

4. 2. Full Symmetry Consideration

The best-fit results using 12 oscillators are given in Figure 9, while the corresponding parameters in Table 2. The band width of the ν_{as}OH mode is much narrower as in the measured spectra. This is particularly visible on the higher frequency end (very low reflectance in the region from 1000 to 1200 cm⁻¹). In order to be able to take into account that $\Omega_{LO} < \Omega_{TO}$ for bands with shape of Evans holes, the $\Delta\varepsilon$ was allowed to obtain negative values during the fitting procedure (cf. equation 10). The band with frequency at 900 cm⁻¹ was fitted under condition for Evans hole ($\Delta\varepsilon < 0$) and the fitting result proves this finding. Quite similar profile of the reflectance band (resembling a dip) can be achieved if negative values for the damping are allowed. The bands with transversal frequencies at 1506 cm⁻¹ and 1205 cm⁻¹ are such cases, meaning that they simulate Evans type of hole, although the model function does not correspond to such a case. However, the characteristic band shape of Evans holes appearing on the broad ν_{as}OH mode are again not quite well reproduced. The reason for the second lack of correspondence is probably the rather narrow OH stretching band.
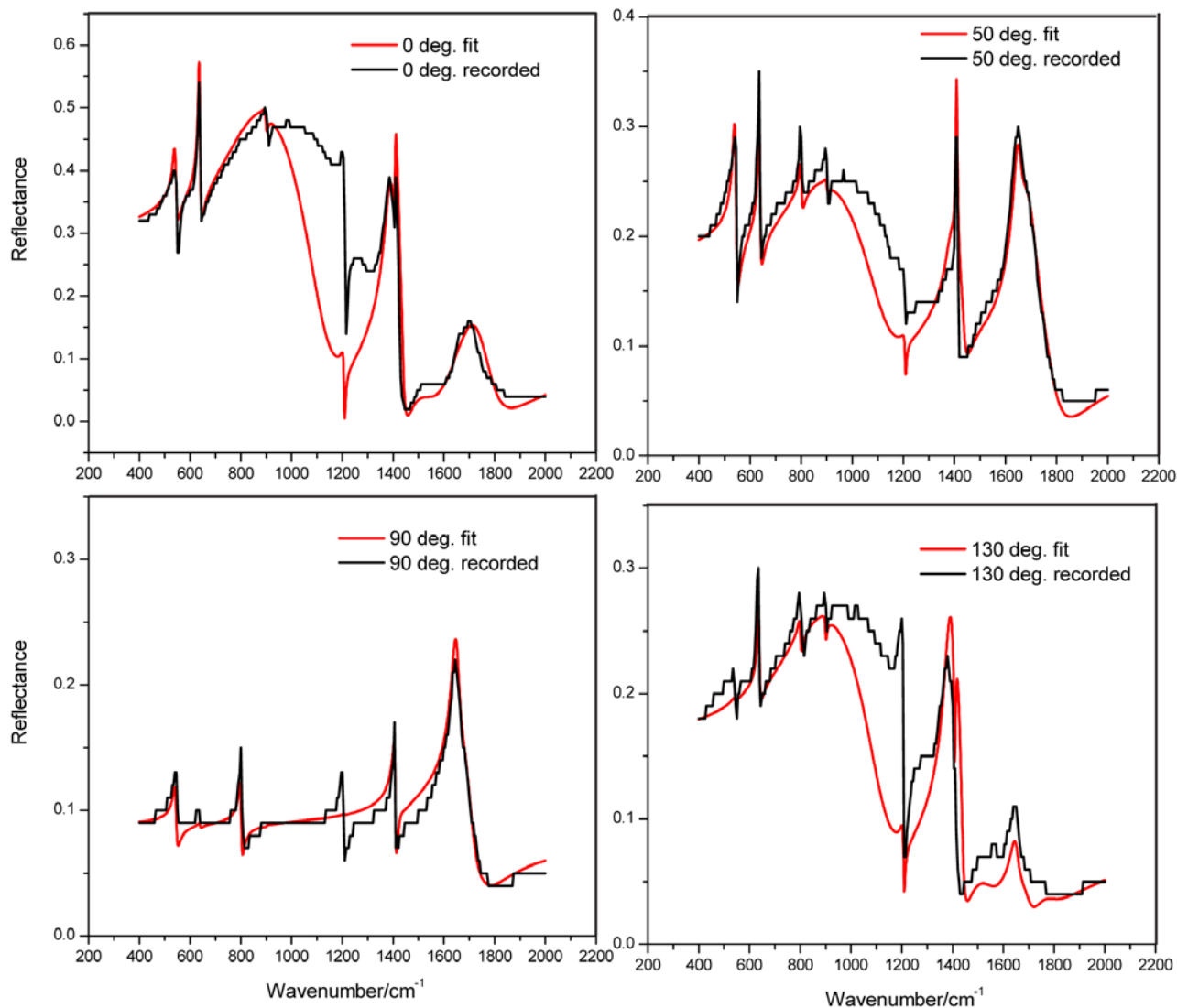
Figure 9. Fitted reflectance spectra for the four angles of polarization: 0°, 50°, 90° and 130°, presented together with the measured one, employing twelve oscillators.

Table 2. B_u-phonon parameters obtained from the best-fit dispersion analysis using twelve oscillators.

Assignment	Ω_{TO} (cm⁻¹)	$\Delta\varepsilon$	γ (cm⁻¹)	θ (°)
	1694	0.237	174	10
	1676	0.126	80	62
νC=O	1645	0.090	32	71
δOH	1506	0.285	–251	172
δCH₂	1407	0.027	6	39
νC-O	1380	0.275	40	170
wag CH₂	1205	0.024	–10	175
νC-C	900	–0.019	10	172
ν_{as}OH	838	4.414	250	179
rock CH₂	800	0.020	10	70
δOCO	634	0.280	6	4
πC=O	539	0.266	12	20
	$\varepsilon_{\infty xx} = 4.68$	$\varepsilon_{\infty zz} = 3.16$	$\varepsilon_{\infty xz} = 0.22$	

One has to be careful with the obtained ε_∞ values. The reflectance data are available up to 2000 cm⁻¹, above which the bands due to the CH₂ stretchings are present that have not been taken into account in the fitting procedure. As previously explained, the oscillator strength of the dielectric constant due to these vibrations contributes to the ε_∞ value, as stated by equation (7). Thus, the fitted values for ε_∞ are only local parameters and can not be addressed as high-frequency dielectric constants.

In order to obtain better fit, an extra oscillator was added in the region of the broad ν_{as}OH stretching. To assure that bands with small intensity will not be omitted from the calculation due to the vicinity of a strong band, some of the vibrational parameters were intentionally fixed. For this purpose we have chosen some of the parameters of the bands at 900 cm⁻¹ and 800 cm⁻¹ to be fixed. The
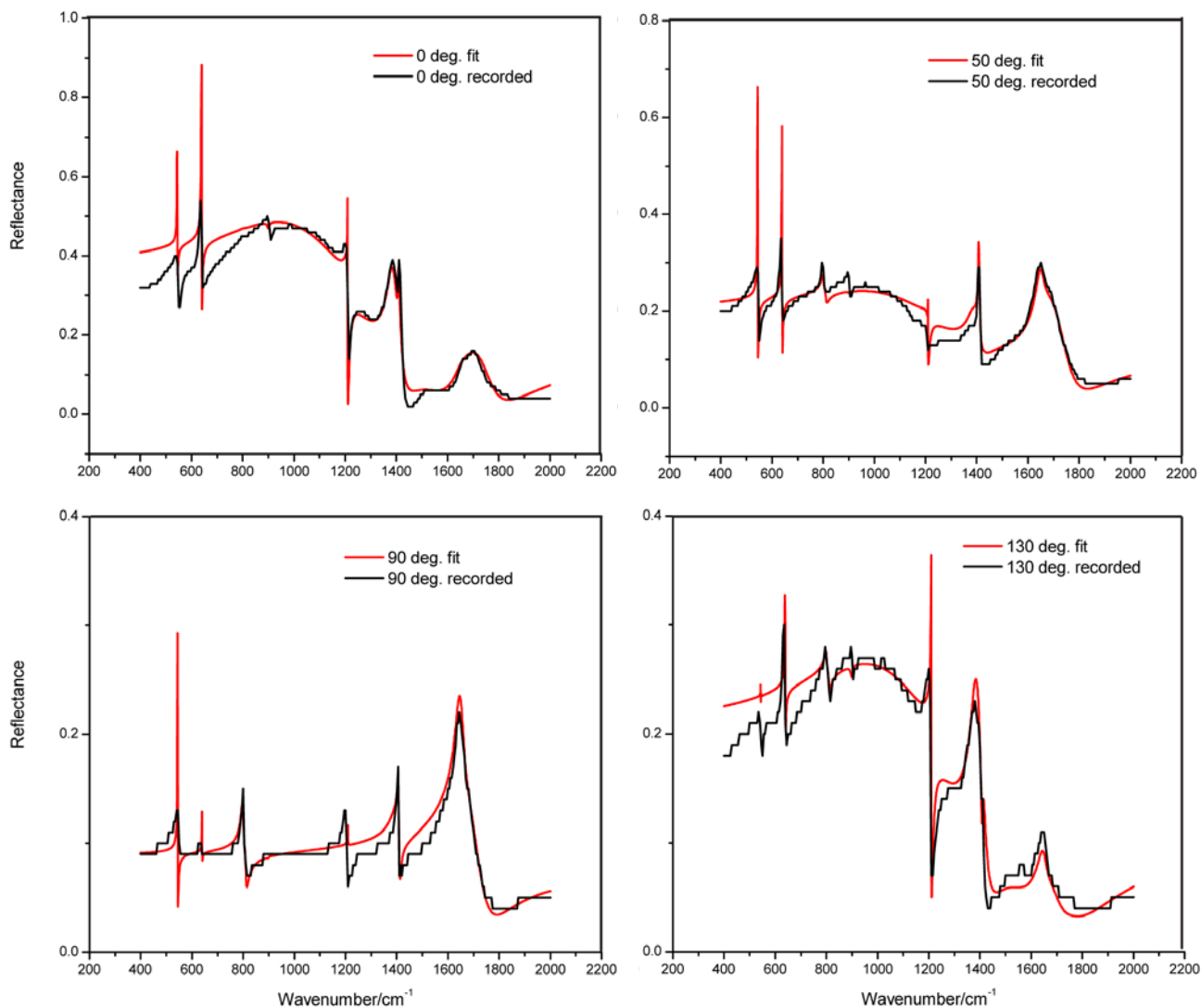
Figure 10 Fitted reflectance spectra for the four polarization angles: 0°, 50°, 90° and 130° presented together with the measured one, employing thirteen oscillators.

results obtained in this way are presented in Figure 10, while the obtained phonon mode parameters are given in Table 3. Much better fit of the calculated spectrum to the four measured reflectance spectra was obtained when using additional oscillators (cf. Figures 9 and 10).

4. 3. Comparison of the Results

The three calculations give similar results. The values of transition dipole moments directions (θ) are in phenomenological model only rough data, but the full symmetry consideration gives more precisely defined values. However, the results of both methods are very similar except some discrepancies for some modes. Similar vibrational frequencies of phonon modes (Ω_{TO}) were also obtained. All basic spectral features were described in phenomenological and in full symmetry consideration with 13 oscillators.

Table 3. B_u-phonon parameters obtained from the best-fit dispersion analysis using one additional oscillator (frequency at 808 cm^{-1}).

Assignment	Ω_{TO} (cm^{-1})	$\Delta\varepsilon$	γ(cm^{-1})	θ (°)
	1675	0.185	116	62
	1660	0.221	182	178
νC=O	1645	0.086	33	69
δOH	1526	0.789	–360	176
δCH$_2$	1407	0.026	5	39
νC-O	1379	0.204	36	169
wag CH$_2$	1214	–0.168	25	1
ν_{as}OH	947	10.075	482	178
νC-C	900	–0.018	10	172
*	808	0.0130	11	72
rock CH$_2$	800	0.020	10	70
δOCO	637	0.204	–1	4
πC=O	543	0.098	0.4	19

$$\varepsilon_{\infty xx} = 7.18 \quad \varepsilon_{\infty zz} = 3.14 \quad \varepsilon_{\infty xz} = 0.130$$

* additional oscillator

All calculation procedures give very large strength for $\nu_{as}OH$, which is up to 100 time larger than the next largest $\Delta\varepsilon$. However, quite different TO-mode frequencies were obtained in full symmetry consideration, 838 cm^{-1} and 947 cm^{-1} (12 and 13 oscillators respectively) and 860 cm^{-1} by the phenomenological approach. All three calculations give very large damping of the $\nu_{as}OH$. In phenomenological approach the γ_{TO} damping has to be applied in such a comparison. However, certain asymmetry of this mode was obtained (γ_{LO}/γ_{TO} = 1.15, see Table 1). All three calculations give almost the same direction of $\nu_{as}OH$ transition dipole moment.

The phenomenological approach address two Evans holes, the $\nu(C–C)$ at 911 cm^{-1} and wag CH$_2$ at 1212 cm^{-1} (Table 1). They are characterized by $\Omega_{TO} < \Omega_{LO}$ which causes negative strength of these modes ($\Delta\varepsilon < 0$). Both bands are asymmetrical, where the asymmetry of the band at 1212 cm^{-1} is extremely large. The full symmetry consideration fits the parameters of the dielectric function to unusual band shapes using negative dampings and negative strength. In principle, both approaches can produce spectral holes, that is confirmed by the parameters of $\nu(C–C)$ and wag CH$_2$ bands which were obtained using 12- and 13-oscillator fits (Tables 2 and 3). Interestingly, the dampings and transition dipole moment directions of both modes are very similar in all three calculations.

The band assigned as δOH was described in phenomenological approach with large asymmetry (γ_{LO}/γ_{TO} = 1.5, see Table 1) and in full symmetry consideration with negative damping (Tables 2 and 3). It is very likely that negative damping constant reveal asymmetric reflectance band which the three-parametric dispersion relation cannot account for. It is worth point out here that the direction of transition dipole moment of this band is very similar in all the three calculations.

5. Conclusions

Model calculations of near-normal incidence bulk reflectance spectra show how different band shapes could be described by oscillator parameters of dielectric function. Most interesting situation is the case of the so-called Evans holes. A weak oscillator appearing within the frequency region of a strong one (i.e. between its TO and LO frequencies) shifts LO-mode frequency to wavenumbers higher than its TO-mode frequency. This gives rise to negative oscillator strength of the weak mode and a remarkable reflectance dip (Evans hole) in reflectance spectrum. This model was applied in analysis of bulk reflectance spectra of a monoclinic crystal with strong hydrogen bond.

The specular reflectance spectra of KHSu monocrystal measured in *ac* crystal plane were studied in particular. Two approaches were applied to solve the symmetry

issues of dielectric tensor for each oscillator, a phenomenological and full symmetry consideration.

The so-called phenomenological one, apply the four-parametric model for dielectric function. It gives four data for each vibrational mode, the frequency and damping of the TO- and LO- phonon modes which further allows calculation of oscillator strengths. The benefit of this model is in the possibility to evaluate asymmetric reflectance bands. This is the main reason for very good fit of the model to all B$_u$-mode reflectance spectra. The monoclinic symmetry was taken into account phenomenologically. The parameters of B$_u$-normal vibrations were selected applying the dependence of oscillator strengths on polarization angle in the *ac* crystal plane. A cosine dependence was obtained for many bands, including all bands with larger oscillator strength. Such dependence is valid for orthorhombic symmetry where *a* and *c* axis are perpendicular. KHSu crystal approximately satisfy this condition (β = 90.8°) which is the reason why the applied method works well. The phonon frequencies, dampings and transition dipole angle for such an oscillator could be adequately obtained at the polarization angle where the corresponding oscillator strength is maximal.

The full symmetry consideration takes into account real description of dielectric tensor for the *ac* plane of monoclinic symmetry. This description needs to fit all the parameters to more reflectance spectra simultaneously; four reflectance spectra were used here. The calculation applies the three-parameter model for dielectric function. This model could not reproduce bands with larger asymmetry. This is the most probable reason for troubles with fitting the reflectance spectrum of KHSu. It was solved with additional (fictive) oscillator which helps to obtain wide reflectance band of the $\nu_{as}OH$ vibration. Some of the bands needed negative values for damping in order to reproduce the band shape. In four-parametric dielectric function model, such a shape is described by different TO and LO dampings. The real advantage of the model is that it gives precise values of directions of transition dipole moment, contrary to the phenomenological model which could provide for only a rough estimation.

Both approaches describe well all basic spectral features, the wide reflectance of $\nu_{as}OH$ and the two Evans holes appearing for weak bands located on its shoulder.

6. Acknowledgements

7. References

1. M. Born and K. Huang, Dynamical Theory of Crystal Lattices, Clarendon Press, Oxford, **1968**.

2. P. M. A. Sherowood, Vibrational Spectroscopy of Solids, Cambridge University press **1972**.

3. S. S. Mitra, E. D. Palik (Ed.): Handbook of optical constants of solids, **1985**, Academic Press, pp. 213–270.

4. Y. Luspin, J. L. Servoin, F. Gervais, *J. Phs. C: Sol. St. Phys.* **1980**, *13*, 3761–3773

5. F. Gervais, Y. Luspin, J. L. Servoin, *Ferroelectrics* **1980**, *24*, 285–288

6. J. L. Servoin, F. Gervais, A. M. Quittet, Y. Luspin, Phys. Rev. B **1980**, *21*, 2038–2041

7. J. L. Servoin, Y. Luspin and F. Gervais, Phys. Rev. B **1980**, *22,* 5501

8. A.S. Barker, Phys. Rev. **1966**, *146*, 391–399

9. F. Gervais, B. Piriou, Phys. Rev. B **1974**, *10*, 1642

10. F. Gervais, B. Piriou, J. Phys. C: Sol. St. Phys. **1974**, *7*, 2374

11. F. Gervais J.F. Baumard, Sol. St. Commun. **1977**, *21*, 861

12. F. Gervais, B. Piriou, Phys. Rev. B **1975**, *11*, 3944

13. W. G. Spitzer, D. A. Kleinman, Phys. Rev. **1961**, *121*, 1324

14. F. Gervais, B. Piriou, F. Cabannes, Phys. Stat. Sol. B **1972**, *51*, 701

15. R. Claus, L. Merten, J. Brandmüller, Springer Tracts in Modern Physics **1975**, *74*, 1–237

16. H. T. Flakus, Chem. Phys. **1981**, *62*, 103

17. D. Hadži, B. Orel, Vibrational spectra of mercaptobenzolthiazole, unpublished results (1978)

18. S. Detoni, D. Hadži, B. Orel, J.Bournay in Proceedings of the 2nd Workshop in dynamics of hydrogen bond in solids and liquids – Horizons in hydrogen bond research, Munich 1978.

19. L. Angeloni, M.P. Marzocchi, D. Hadži, B. Orel, G. Sbrana, Spectrochimica Acta A **1977**, *33*, 735–744

20. D. Hadži, B. Orel, Indian Journal of Pure and Applied Physics **1978**, *16*, 376–384

21. L. Angeloni, M.P. Marzocchi, S. Detoni, D. Hadži, B. Orel, G. Sbrana, Spectrochimica Acta A **1978**, *34*, 253–261

22. D. Hadži, I. Leban, B. Orel, M. Iwata, J. M. Williams, J. Cryst. Mol. Struct. 9 (1979) 117

23. B. Orel, D. Hadži, M. Janežič, unpublished results (1980)

24. D. Hadži, B. Orel, A. Novak, Spectrochimica Acta A **1973**, *29*, 1745–1753

25. L. Angeloni, M.P. Marzocchi, D. Hadži, B. Orel, G. Sbrana, Chem. Phys. Lett. **1974**, *28,* 201–204

26. J. C. Evans, Spectrochimica Acta **1960**, *16*, 994–1000

27. T. Kurosawa, J. Phys. Soc. Jpn. **1961**, *16*, 1298–1308

28. M. Klanjšek Gunde, B. Sc. Thesis, Ljubljana, **1982**.

29. M. Klanjšek Gunde, Appl. Spectrosc. **1992**, *46*, 365–372.

30. H. Kuzmany: Solid State Spectroscopy. An Introduction, Springer-Verlag Berlin, Heidelberg **1998**.

31. V. M. Schreiber, D. N. Shchepkin, T. V. Sokornova, J. Mol. Str. **1994**, *322*, 217–221.

32. R. Claus, Phys. Stat. Sol. b **1978**, *88*, 683–688.

33. R. Claus, Phys. Stat. Sol. b **1980**, *100*, 9–41.

34. V. Ivanovski, Th.G. Mayerhöfer, J. Popp, V. Petruševski, Spectrochim. Acta A **2008**, *69* 629–641.

35. M. V. Belousov, V. F. Pavinich, Opt. Spectrosc. **1978**, *45*, 771–774

36. J. R. Aronson, A. G. Emslie, E. V. Miseo, E. M. Smith and P. F. Strong, Appl. Opt. **1983**, *22*, 4093–4098

37. V. Ivanovski, Th. G. Mayerhöfer, J. Popp, Vibrat. Spectrosc. **2008**, *47*, 91–98.

38. V. Ivanovski, Th. G. Mayerhöfer, J. Popp, Vibrat. Spectrosc. **2007**, *44,* 369–374.

39. A. B. Kuz`menko, E. A. Tischenko, V. G. Orlov, J. Phys.: Condens. Matter, 8 (1996) 6199–6212.

40. Mathematica for Windows, Version 5.2, Wolfram Research Inc., 2005.

Povzetek

Spektralna odbojnost monokristalov ima lahko zelo različne in zanimive oblike; mednje sodijo zlasti Evansove luknje. Take oblike smo opisali z modelnim računom z uporabo dielektrične funkcije. Kadar se šibak oscilator pojavi na frekvenčnem območju močnega oscilatorja (to je med njegovima TO in LO frekvencama), se LO-frekvenca šibkega oscilatorja pomakne k višjim frekvencam, preko njegove TO-frekvence. Oscilatorska moč takega nihanja je negativna, kar povzroči padec odbojnosti in s tem Evansovo luknjo v spektru. Ta model smo uspešno uporabili za analizo TE-polariziranega spektra odbojnosti monokristala kalijevega hidrogen sukcinata v *ac* kristalni ravnini. Monoklinsko kristalno simetrijo smo opisali z enostavnim fenomenološkim modelom in s kompletno simetrijsko analizo. Pri fenomenološkem opisu smo uporabili štiri-parametrični model dielektrične funkcije. Ta omogoča zelo dober opis oblike trakov v vseh spektrih, tudi asimetričnih. Oscilatorske moči nekaterih trakov so kosinusno odvisne od polarizacijskega kota, kar je posledica zelo majhne razlike monoklinskega kristalnega kota od ortorombskega. Zaradi tega fenomenološki opis daje dobre parametre za večino nihanj v spektru. Kompletna simetrijska analiza opiše nihanja v *ac* ravnini z dielektričnim tenzorjem, v njegovih lastnih smereh pa uporablja tri-parametrični model za dielektrično funkcijo. Tak opis daje zelo dobre rezultate za smeri dipolnih momentov, vendar slabše opiše oblike trakov v spektrih. Obe aproksimaciji opišeta vse osnovne spektralne oblike, široki trak zaradi $v_{as}OH$ in obe Evansovi luknji na njegovih ramenih.